Hyperspectral imaging to measure apricot attributes during storage

Alessandro Benelli,[1] Chiara Cevoli,[1,2] Angelo Fabbri,[1,2] Luigi Ragni[1,2]

[1]Department of Agricultural and Food Sciences; and [2]Interdepartmental Centre for Agri-Food Industrial Research, Alma Mater Studiorum, University of Bologna, Cesena (FC), Italy

Abstract

The fruit industry needs rapid and non-destructive techniques to evaluate the quality of the products in the field and during the post-harvest phase. The soluble solids content (SSC), in terms of °Brix, and the flesh firmness (FF) are typical parameters used to measure fruit quality and maturity state. Hyperspectral imaging (HSI) is a powerful technique that combines image analysis and infrared spectroscopy. This study aimed to evaluate the potential of the application of the Vis/NIR push-broom hyperspectral imaging (400 to 1000 nm) to predict the firmness and the °Brix in apricots (180 samples) during storage (11 days). Partial least squares (PLS) and artificial neural networks (ANN) were used to develop predictive models. For the PLS, R^2 values (test set) up to 0.85 (RMSEP=1.64 N) and 0.72 (RMSEP=0.51 °Brix) were obtained for the FF and SSC, respectively. Concerning the ANN, the best results in the test set were achieved for the FF (R^2=0.85, RMSEP=1.50 N). The study showed the potential of the HSI technique as a non-destructive tool for measuring apricot quality even along the whole supply chain.

Correspondence: Chiara Cevoli, Department of Agricultural and Food Sciences, Alma Mater Studiorum, University of Bologna, Piazza Goidanich 60, 47521 Cesena (FC), Italy.
E-mail: chiara.cevoli3@unibo.it

Key words: Apricot; storage; hyperspectral imaging; artificial neural networks; partial least squares.

Conflict of interest: the authors declare no potential conflict of interest.

Received for publication: 15 November 2021.
Accepted for publication: 15 April 2022.

Journal of Agricultural Engineering 2022; LIII:1311
doi:10.4081/jae.2022.1311

Introduction

The optimal harvest time or the right degree of ripeness of apricots (*Prunus armeniaca* L.) intended for the fresh market are typically determined by measuring the fruit's chemical and physical quality parameters, *i.e.*, the ripening indexes. The measurement of the quality parameters of the fruit is traditionally carried out using destructive analytical techniques, which also involve long operating times (Witherspoon and Jackson, 1995). In the last decades, numerous researches have been addressed the fast and non-destructive estimation of fruit ripening indexes through spectroscopic methods, including near- and mid-infrared spectroscopy (NIR/MIR); in particular, for apricots have been analysed: soluble solids content (SSC), titratable acidity (TA), flesh firmness (FF), total carotenoids content (TCC), total phenolic content (TPC) and flavonols content (FLC) (Carlini *et al*., 2000; Manley *et al*., 2007; Ruiz *et al*., 2008; Bureau *et al*., 2009; Camps and Christen, 2009a; Camps and Christen, 2009b; Berardinelli *et al*., 2010; Bureau *et al*., 2012; Christen *et al*., 2012; De Oliveira *et al*., 2014; Buyukcan and Kavdir, 2017; Amoriello *et al*., 2018; Bureau *et al*., 2018; Ciacciulli *et al*., 2018; Amoriello *et al*., 2019; Guo *et al*., 2019). Another spectroscopic technique that has been increasingly applied in the last decade to determine fruit and vegetable quality parameters is hyperspectral imaging (HSI). HSI combines image analysis and spectroscopy, in particular Vis/NIR spectroscopy. HSI allows to obtain as many absorbance/reflectance/transmittance spectra as there are single acquired pixels (in this technique called voxels) that form the hyperspectral image; the output is a hypercube, composed of data with two spatial and a spectral dimension. This method of analysis is fast and non-destructive, without the need for contact with the sample to be analysed. HSI is applied for the determination of quality parameters of fruit and vegetables both directly in the field and in the laboratory. The processing of the acquired hyperspectral images generally requires several steps: the use of hyperspectral image segmentation techniques, in order to reduce the size of the acquired data; the application of a region of interest (ROI) selection method, from which the hyperspectral data required can be derived; finally, the application of spectra pre-treatment techniques for the implementation of multivariate data analysis. Partial least square regression (PLS), supporting vector machines (SVM) and artificial neural networks (ANN), are popular multivariate regression techniques used for hyperspectral imaging.

There are several studies on the determination of fruit quality parameters through HSI (Chandrasekaran *et al*., 2019), but there is only one study concerning apricots (Xue *et al*., 2015). The authors evaluated the ripeness of the *Shajin* apricot, in terms of 4 ripeness classes (unripe, mid-ripe, ripe, and over-ripe according to the days after harvesting) and SSC, by using the HSI in the band range of 400-1000 nm. The extreme learning machine (ELM) was used as a classification technique. The results showed a correct discrimination rate of 93.33%, but regression models able to estimate the

SSC have not been developed.

In this study, the potential of the HSI technique combined with multivariate data analyses (PLS and ANN) to non-destructively predict quality parameters (SSC and FF) of apricots in post-harvest conditions was investigated. This would allow assessing the degree of ripeness of the fruit suitable for the fresh market.

Materials and methods

Samples

180 samples of apricot c.v. *Farbaly* harvested in July 2019 in the Cesena area (Italy) and stored at 4°C were used for the research. The analyses were carried out after 1 (I), 2 (II), 3 (III), 4 (IV), 5 (V), 8 (VI), 9 (VII), 10 (VIII), and 11 (IX) days of storage at 20 °C, for a total of nine storage times. Twenty apricots for storage time were evaluated. These storage conditions have been chosen to reproduce those in the fresh market.

Hyperspectral measurements

The hyperspectral (HS) images of the apricots were obtained through the use of a push-broom linear array hyperspectral camera (HSC) working in the spectral range from 400 to 1000 nm (Nano-Hyperspec VNIR, Headwall Photonics, Inc., Fitchburg, MA, USA) with a 17 mm EFL (effective focal length) lens. The HSC scans one line of voxels at a time, with a spatial resolution of 640 points, each characterised by 272 spectral bands, with a nominal spectral resolution of 2.2 nm. The HSC has been set with an exposure and frame period of 25 ms: the frame rate is a variable depending on the set exposure time; in this case, it was 34.22 frames per second (FPS).

The set-up used during the experimental test is shown in Figure 1. Remarkably, the HSC has been mounted on a metallic frame with the optical axis perpendicular to the underlying conveyor belt, on which the sample runs, at the height of 54 cm. The conveyor belt speed has been set to 8 mm s^{-1}. On the same frame, two halogen spotlights with 120 W lamps have been mounted, inclined by 15° as compared to the conveyor belt plane and at the height of 32 cm. The analysis was carried out by isolating the apparatus from the external light using a correctly assembled box. The hyperspectral image was obtained by progressive scanning several lines, keeping the HSC fixed, and running the sample on a prototype conveyor belt, which simulates an industrial fruit sorting line.

The reflectance spectrum of white reference (R_W) was obtained respectively utilising a white cardboard sheet covering the entire angle of view of the HSC; the reflectance spectrum of dark reference (R_D) was obtained by placing the cover on the lens. The scan of the sample obtained raw diffuse reflectance spectrum (R_R). The calibrated diffuse reflectance spectrum (R_C) was calculated by the following equation (Guo *et al*., 2019):

$$R_C = \frac{R_R - R_D}{R_W - R_D} \quad (1)$$

Each whole apricot was longitudinally scanned twice, one per side. The sample temperature was 23±1°C.

Destructive measurements of quality parameters

The quality parameters (FF and SSC) were measured immediately after acquiring the HS images. The apricots were prepared for FF analysis by cutting them in half with a knife along the longitudinal plane, depriving them of the kernel, and finally removing the concavity resulting from the removal of the kernel in order to obtain a flat support surface. FF (N) was determined on each half portion of the fruit on the equatorial area by a compression test performed with a texture analyser (TA-HDi, Stable Micro System Ltd., Godalming, UK) during a penetration of 9 mm obtained by a 6 mm diameter flat-headed cylindrical steel probe mounted on a 50 N load cell. The test speed was 0.5 mm s^{-1}. The SSC (°Brix) was measured through a digital refractometer (PR-101 Digital Refractometer, ATAGO CO., LTD, Tokyo, Japan) on juice obtained from the pulp in the equatorial area of the fruit side previously analysed with the texture analyser (Witherspoon and Jackson, 1995). An average value of the ripening index was subsequently obtained by averaging the FF and °Brix grade values of the two sides of the fruit. Significant differences between the means of the quality parameters at different storage times were evaluated through analysis of variance (ANOVA with Tukey-HSD post-hoc test, p-level<0.05). In the case of non-homogeneity of variance, evaluated by the Levene test, the non-parametric Kruskal-Wallis test (p-level<0.05) with multiple comparison z' post-hoc test (Dunn's test) was applied.

Multivariate data analysis

For each sample side, a mean spectrum was calculated by averaging the spectra of the region of interest (ROI), a selected equatorial area measuring 30×30 voxels (900 spectra). This operation was done using HyperCube v. 11.52 software (U.S. Army Engineer Research and Development Centre (ERDC), USA). The mean spectra of the two sides were averaged and used for the chemometric elaborations. Principal component analysis (PCA) was used as

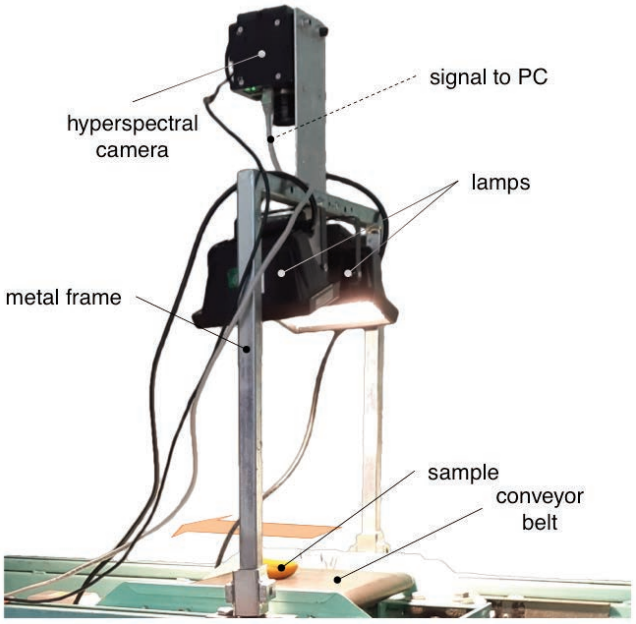

Figure 1. Components of the hyperspectral imaging system developed for the experiment.

an explorative technique to evaluate the spectra variations and identify sample outliers. Two different statistical techniques were used to predict SSC and FF: the first (PLS) based on a linear approach and the second (ANN) on a non-linear approach. The dataset was split into two sub-sets, one to train and cross-validate the models (80% of the entire dataset) and the other (20%) to external validate it (test set) by using the Kennard-Stone method (selects samples that best span the same range as the original data, but with an even distribution of samples across the same range). The overfitting of the models was avoided by monitoring the root mean square error in cross-validation (RMSECV) as a function of the latent variables (PLS) or iterations number (ANN). Variable importance in the projection (VIP) method was adopted to identify and select relevant variables. VIP scores estimate the relevance of each predictor in the projection used in a PLS model: since the mean of squared VIP scores is equal to 1, and the 'greater than one' rule is frequently used as a variable selection criterion (Chong and Jun, 2005). Finally, the results were expressed in terms of R^2, root mean square error (RMSE), and residual prediction deviation (RPD), defined as the standard deviation of observed values divided by the RMSE: a good model should have a high R^2, a low RMSE, and a high RPD.

PLS regression models were developed by using PLS Toolbox for Matlab2018a®. Spectral bands between 400 and 426 nm (13 spectral bands) and between 980 and 1000 nm (11 spectral bands) were excluded due to the low signal-to-noise ratio generated by the hyperspectral sensor as also observed by Wendel *et al*. (2018). The spectra were pre-treated with standard normal variate (SNV) or Savitzky-Golay first derivative (D1) transformation (10 points) and finally mean centred (MC) to improve the prediction performance.

The ANN models were performed using the Neural Net Fitting tool for Matlab2018a®. Specifically, two multi-layer perceptron (MLP) neural networks were built to predict SSC and FF. A linear activation function was used for input and output layers, while for the hidden layer, a logistic activation function was applied. Given that the ANN ability should capture an implicit pre-processing of the spectra (Helin *et al*., 2021), the raw spectra were only subjected to denoising (Savitzky-Golay method with 15 smoothing points). Furthermore, the software independently applies min-max normalisation to speed up learning and lead to faster convergence.

Looking for the best classification ability, different node numbers in the hidden layer and combinations were tested. The ANNs were trained by using the Levenberg-Marquardt backpropagation method.

Results and discussion

The mean and standard deviation values of SSC and FF are shown in Table 1. The obtained values are in agreement with those reported by Ciacciulli *et al*. (2018), Berardinelli *et al*. (2010), and Manley *et al*. (2007) for apricots analysed during different days of storage. Significant differences emerged for both FF and SSC between measurements at different storage times.

The range of variation of FF is relatively high, with a decrease from the day I to the day IX of 79%. However, in the same period, SSC increased by 9%.

Raw spectra and pre-treated spectra by the first derivative of all the samples by day of analysis are shown in Figure 2. The Vis/NIR region from 400 to 1000 nm is characterised by vibration overtones and combination bands of O–H, C–H, and N–H bonds related to the principal structural organic molecules (Manley *et al*., 2007). In the visible spectrum (400-700 nm) are present the absorption bands of substances used as ripening indexes of fruit (Manley *et al*., 2007). For example, the absorption band of anthocyanins is around 500 nm (ElMasry *et al*., 2007), the range of absorption bands related to carotenoids is between 570 and 590 nm (Munera *et al*., 2017), and between 680 and 710 nm for chlorophyll-α (McGlone and Kawano, 1998; ElMasry *et al*., 2007; Pu *et al*., 2016; Munera *et al*., 2017; Amoriello *et al*., 2018).

Table 1. Means and standard deviations (in brackets) of maturity indices as a function of storage time (n=20 for each storage time).

Storage time	SSC (°Brix)	FF (N)
I	15.0^{a} (1.0)	14.3^{a} (2.8)
II	15.7^{a,b} (0.9)	13.0^{a} (3.4)
III	16.5^{b,c} (1.4)	10.2^{a,b} (1.7)
IV	16.4^{b,c} (0.7)	8.3^{a,b,c} (1.4)
V	16.6^{b,c} (0.8)	6.6^{b,c,d} (0.8)
VI	16.6^{b,c} (0.6)	4.0^{c,d,e} (0.4)
VII	17.0^{c} (0.8)	3.5^{d,e} (0.6)
VIII	16.5^{b,c} (0.7)	3.4^{e} (0.6)
IX	16.4^{b,c} (0.9)	3.0^{e} (0.6)

Differences between means with the same letter are not significant at P<0.05. SSC, soluble solids content; FF, flesh firmness.

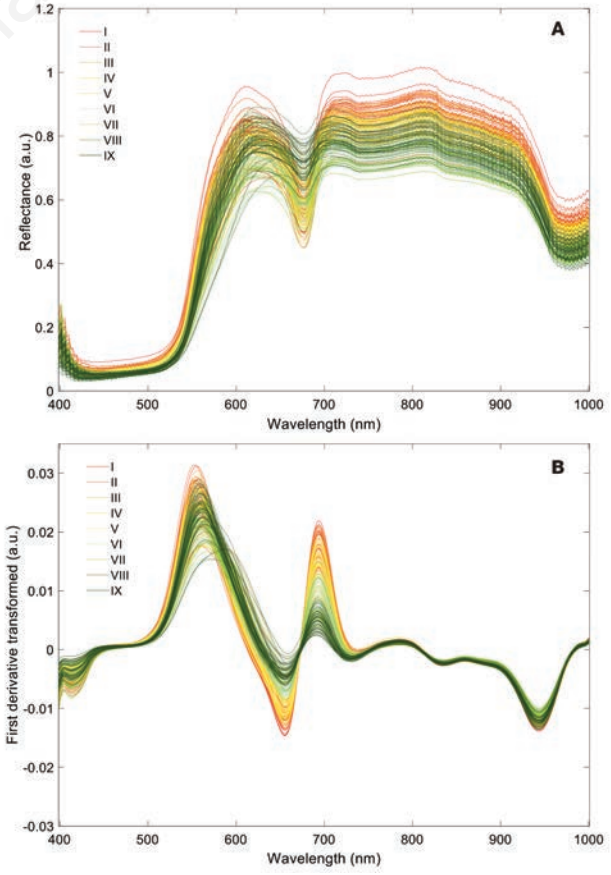

Figure 2. Raw spectra (A) and first derivative (B) of all samples on different days (from I to IX) of analysis.

Absorption bands related to water with an overtone of O–H bonds were observed at 760 nm (Nicolaï *et al*., 2007) and 970 nm (Nicolaï *et al*., 2007; Bureau *et al*., 2009). Following the latter statement, a strong absorption band related to water was observed at around 960 nm (McGlone and Kawano, 1998; Pu *et al*., 2016; Guo *et al*., 2019) and can be expected to prevail since the water content of the fresh fruit is 80-90% (McGlone and Kawano, 1998). In general, the water absorption peaks in the spectral region between 700 and 1000 nm are less marked and wide. Therefore, the spectral information from substances present in the fruit at low concentrations will tend to be less covered by the presence of water (Manley *et al*., 2007). Absorbance peaks were observed between 950 and 1000 nm for carbohydrates and water, corresponding to the second overtone of O–H and N–H, a combination band of O–H bonds, and the third overtone of C–H (Camps and Christen, 2009a). Absorption regions at 840 nm have been indicated as probable sugar absorption bands (Pu *et al*., 2016). In summary, regions within the 800-1000 nm range have been related to SSC variations, while absorption bands referred to water have been located at 960-970 nm (Camps and Christen, 2009b).

The variance between the spectra acquired at different storage times was evaluated through PCA. Two different PCAs were developed, the first one by using the spectra pre-treated by SNV+MC and the second one by applying the D1+MC. The score plots of the first two PCs (76.38% and 13.43%; 62.90% and 17.96%) are reported in Figure 3A and B. For both cases, a clear separation of the samples according to all the days of storage is not evident, but the samples are placed from right to left along the PC1 and from bottom to top along the PC2, passing from the time one to time nine. The loading plots (Figure 3C and D) suggest that the discrimination might be attributed to absorption bands related to carotenoids (around 560-590 nm) and chlorophyll-α (around 680-690 nm).

PLS and ANN models were developed to predict FF and SSC. PLS results, in terms of R^2, RMSE, RPD, and number of latent variables (LV), in calibration, cross-validation, and test set, are reported in Table 2. The best models were obtained for both quality parameters (FF and SSC) by treating the spectra with the first derivative and mean centring. In particular, for the FF parameter, R^2 in the test set ranging from 0.83 (RMSEP=1.98 N) to 0.85 (RMSEP=1.64 N) was achieved. For SSC prediction, the results are less good in terms of R^2, ranging from 0.68 to 0.72, probably due to the small variation of the measured SSC values; however, good RMSEP values range from 0.59 to 0.51 °Brix were obtained.

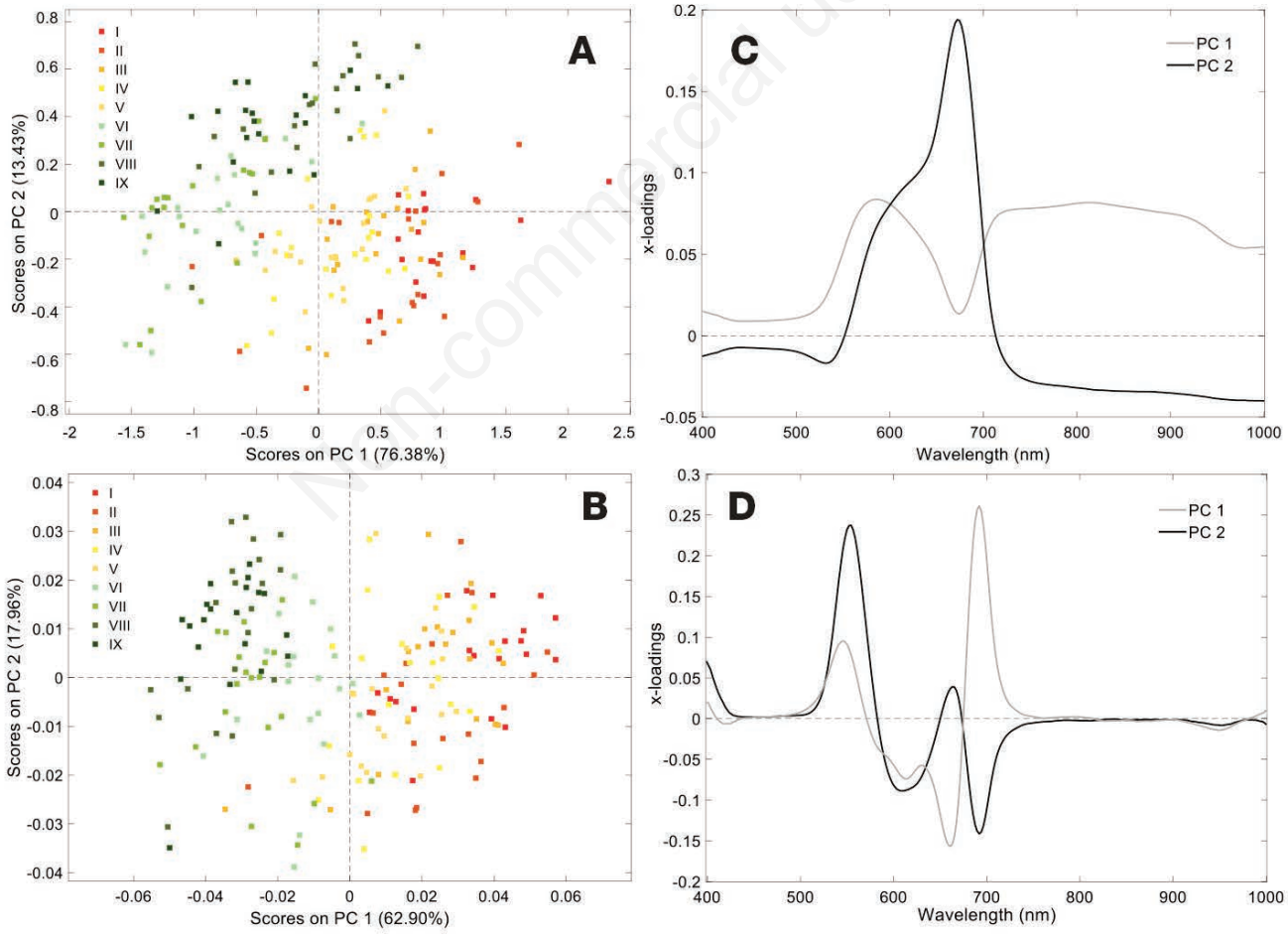

Figure 3. Score plots (A, B) and loading plots (C, D) obtained by principal component analysis (PCA) were developed on all the spectra. Spectra pre-treatments: A, C) standard normal variate and mean centring; B, D) first derivative and mean centring.

RPD values above 2 confirm that the PLS models built to estimate FF are robust; instead, the RPD values calculated for the °Brix models are slightly lower. Figure 4 shows the best results in measured *vs* predicted FF values for the test set.

The spectral and spatial information of each pixel in HS images allows the evaluation of quality parameters of each pixel with chemometric models. The pixels having similar spectra showed similar colours in the images and, consequently, similar predicted values. False colour images were obtained using the best PLS model developed to predict FF. The prediction maps of FF of two representative apricots are shown in Figure 5. The colour bar indicates the scale of the reference values (FF in N). The spatial distribution of FF aligns with the measured values, particularly passing from 2.74 N to 16.53 N; the colour ranges from blue to red. However, the noise of the HS image, influenced by the fruit curvature and inclination of the light source, especially in the peripheral zone, could affect the spectrum of each pixel, which may result in the underestimation of the FF.

The VIP scores obtained by the PLS models built to estimate FF are reported in Figure 6. These scores estimate the importance of each variable in the projection used in a PLS model. A variable with a VIP score close to or greater than one can be considered important in a given model. Considering different spectra pre-treatments (SNV+MC or D1+MC), similar regions with VIP scores higher than one were obtained, suggesting that the wavelengths with the highest contribution to FF prediction range from about 525 to 725 nm. Similar VIP trends were obtained for PLS models developed by using Vis/NIR data and measuring FF and IQI ripening index in peaches and nectarine, respectively (Munera *et al*., 2017; Uwadaira *et al*., 2017).

Regarding ANN, training was repeated five times, and results, in terms of R^2 and RMSE, were averaged since the convergence is

Table 2. Results of partial least squares, in terms of coefficient of determination (R^2), root mean square error (RMSE), residual prediction deviation (RPD) and number of latent variables (LV).

Parameter	Pre-treatment	LV	Calibration set			Cross-validation set			Test set		
			R^2	RMSEC	RPD	R^2	RMSECV	RPD	R^2	RMSEP	RPD
FF (7.3±4.4 N)	SNV+MC	12	0.93	1.16	3.9	0.81	1.99	2.3	0.83	1.98	2.4
	D1+MC	12	0.91	1.39	3.2	0.82	1.85	2.4	0.85	1.64	2.6
SSC (16.3±1.03 °Brix)	SNV+MC	13	0.82	0.42	2.3	0.69	0.58	1.8	0.68	0.59	1.8
	D1+MC	13	0.78	0.46	2.1	0.72	0.50	1.9	0.72	0.51	1.9

SNV, standard normal variate; MC, mean centring; D1, first derivative; FF, flesh firmness; SSC, soluble solids content.

Table 3. Results of artificial neural networks in terms of mean coefficient of determination (R^2), root mean square error (RMSE), and the number of iterations.

Parameter	Training set			Cross-validation set			Test set			Iterations
	R^2	RMSEC	RPD	R^2	RMSECV	RPD	R^2	RMSEP	RPD	
FF (N)	0.95	1.14	4.4	0.86	a	2.6	0.85	1.50	2.6	5
SSC (°Brix)	0.82	0.43	2.4	0.66	0.67	1.7	0.65	0.68	1.7	6

FF, flesh firmness; SSC, soluble solids content.

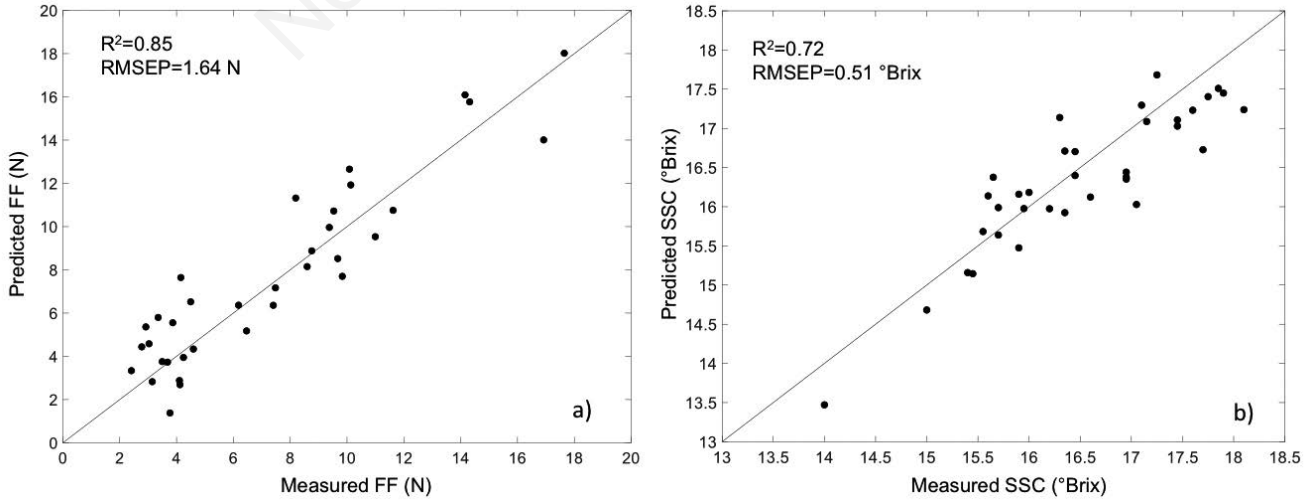

Figure 4. Measured *vs* predicted values of flesh firmness (FF) (A) and soluble solids content (SSC) (B) for the test set, obtained by means of partial least squares (PLS) regression.

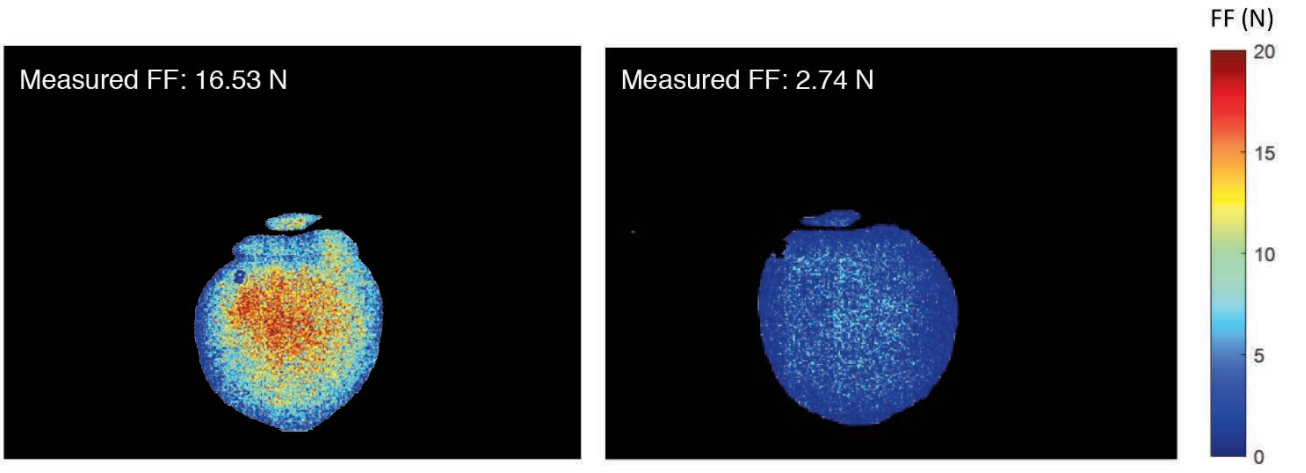

Figure 5. Prediction maps of flesh firmness (FF) of two representative apricots.

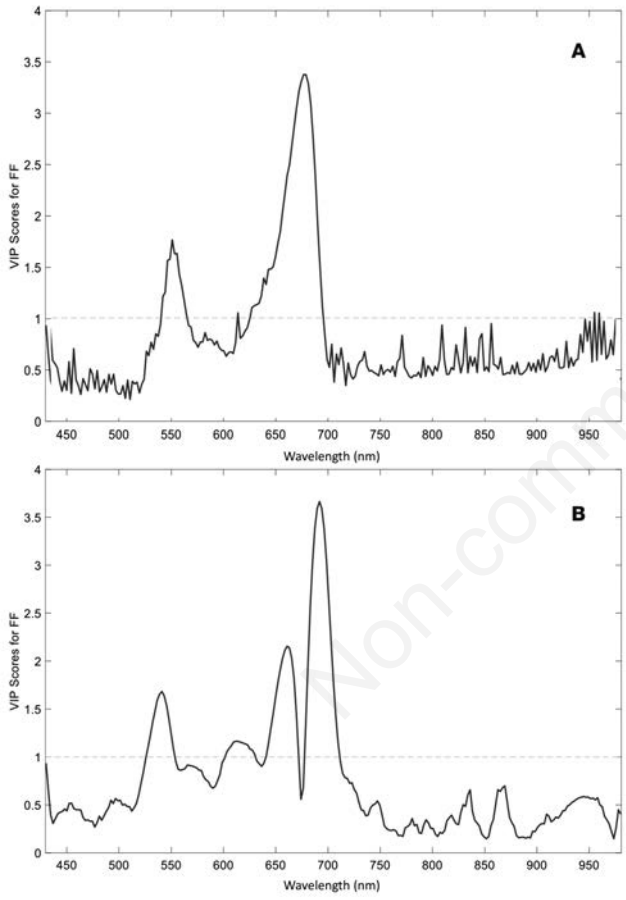

Figure 6. Variable importance in projection (VIP) scores of the partial least squares models to predict flesh firmness (FF). Spectra pre-treatments: A) standard normal variate and mean centring; B) first derivative and mean centring.

influenced by the initial weight values. An early stopping technique was used to select the number of training cycles (iterations) to avoid overfitting, using the validation set to monitor the prediction error. Above this point, the error increased further, indicating that the ANN tends to overfit. An example of the trend of the errors

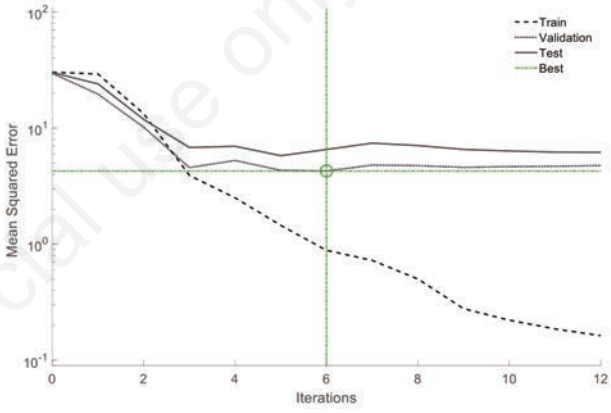

Figure 7. Error graph of training, validation, and test set used to stop the artificial neural networks (ANN) model and select the optimal number of iterations.

(training, validation, and external set) as a function of the iteration number is shown in Figure 7. Finally, the optimal number of iterations (six) was selected, corresponding to the minimum value of the validation error. Over this point, the validation error starts to increase.

The best prediction results were obtained for both the quality parameters with only two nodes in the hidden layer; a more significant number of nodes did not increase the network performance. In terms of R^2, RMSE and number of iterations, in training, cross-validation and test set, the ANN results are reported in Table 3. As for the PLS, the best result in terms of R^2 was achieved for the FF parameter (R^2=0.85, RMSEP=1.50 N). On the other hand, for the prediction of the SSC, R^2 values (0.65 in the test set) lower than those from PLS regression were obtained. A worse performance was also obtained for RMSEP, which was 0.68 °Brix. This is probably due to the slight variation of the measured SSC values during the storage. Also, in this case, RPD values greater than 2 were reached for the prediction of FF.

Comparing the results with those reported in the literature and based on the predictive models built considering a spectral range

comparable with that of this study, it is possible to confirm that R^2 values achieved for the FF parameter are higher or in agreement with those reached in previous works. Camps and Christen (2009a) analysed three apricot varieties by using a portable Vis/NIR spectrometer (650-1200 nm) and reported R values (in validation) between 0.85 and 0.92 for the prediction of the firmness. Camps and Christen (2009b) achieved R values of 0.85 and 0.87 for the Bergarouge and Harostar variety, respectively, considering the same parameters and spectral range. In the former study mentioned (Camps and Christen, 2009a), the SSC prediction resulted in R values between 0.88 and 0.96 (in validation), and RMSECV between 0.67 and 1.00 °Brix. In terms of SSC, the present work results are slightly lower; on the contrary, the range of RMSEP from the PLS models is lower (0.51-0.59 °Brix), which means better performance in RMSEP.

Conclusions

The application of HSI technology allowed us to estimate the FF and SSC of apricots. Two different multivariate techniques were used to build the predictive models. Particularly a linear method (PLS) and a non-linear method (ANN) were tested.

Good and similar results were achieved for the FF parameter by using both the statistical techniques, with R^2 values (test set) of 0.85 for both PLS and ANN and RMSEP of 1.64 N and 1.50 N for the PLS and ANN, respectively. SSC was characterised by a low level of variation (9%) and an initial level already suitable for retail sale: as a possible consequence, both the prediction models (PLS and ANN) were less able to estimate this quality parameter than the previous one (R^2 up to 0.72); nevertheless, RMSEP range obtained by PLS models (0.51-0.59 °Brix) was good. Due to this finding, it would be possible to discriminate and then sort apricots for the fresh market, discarding those with too low FF values and therefore undesirable for retail sale. In light of the obtained results, the HSI technology could be implemented in a sorting line of apricots for the fresh market, subject to the improvement of hyperspectral image segmentation techniques, dimensionality reduction, and finally, prediction to automate real-time analysis.

References

Amoriello T., Ciccoritti R., Carbone K. 2019. Vibrational spectroscopy as a green technology for predicting nutraceutical properties and antiradical potential of early-to-late apricot genotypes. Postharv. Biol. Technol. 155:156-66.

Amoriello T., Ciccoritti R., Paliotta M., Carbone K. 2018. Classification and prediction of early-to-late ripening apricot quality using spectroscopic techniques combined with chemometric tools. Sci. Hortic. 240:310-7.

Berardinelli A., Cevoli C., Silaghi F.A., Fabbri A., Ragni L., Giunchi A. 2010. FT-NIR Spectroscopy for the Quality Characterization of Apricots (Prunus Armeniaca L.). J. Food Sci. 75:462-8.

Bureau S., Reich M., Renard C.M.G.C., Ruiz D., Audergon J.M. 2012. Rapid characterization of apricot fruit quality using near and mid-infrared spectroscopy: Study of the model robustness. Acta Hortic. 934:173-6.

Bureau S., Renard C.M.G.C., Fakhfackh Z., Audergon J.M. 2018. Infrared spectroscopy as a rapid tool to assess apricot fruit quality: Comparison of two strategies for a model establishment. Acta Hortic. 1214:145-9.

Bureau S., Ruiz D., Reich M., Gouble B., Bertrand D., Audergon J.M., Renard C.M.G.C. 2009. Rapid and non-destructive analysis of apricot fruit quality using FT-near-infrared spectroscopy. Food Chem. 113:1323-8.

Buyukcan M.B., Kavdir I. 2017. Prediction of some internal quality parameters of apricot using FT-NIR spectroscopy. J. Food Measure. Character. 11:651-9.

Camps C., Christen D. 2009a. Non-destructive assessment of apricot fruit quality by portable visible-near infrared spectroscopy. LWT - Food Sci. Technol. 42:1125-31.

Camps C., Christen D. 2009b. On-tree follow-up of apricot fruit development using a hand-held NIR instrument. J. Food Agric. Environ. 7:394-400.

Carlini P., Massantini R., Mencarelli F. 2000. Vis-NIR measurement of soluble solids in cherry and apricot by PLS regression and wavelength selection. J. Agric. Food Chem. 48:5236-42.

Chandrasekaran I., Panigrahi S.S., Ravikanth L., Singh C.B. 2019. Potential of near-infrared (NIR) spectroscopy and hyperspectral imaging for quality and safety assessment of fruits: an overview. Food Analyt. Methods. 12:2438-58.

Chong I.G., Jun C.H. 2005. Performance of some variable selection methods when multicollinearity is present. Chemometr. Intell. Lab. Syst. 78:103-12.

Christen D., Camps C., Summermatter A., Gabioud Rebeaud S., Baumgartner D. 2012. Prediction of the pre- and postharvest apricot quality with different VIS/NIRs devices. Acta Hortic. 966:149-54.

Ciacciulli A., Bassi D., Castellari L., Foschi S. 2018. Fruit ripening evolution in diverse commercial apricots by conventional and non-destructive methods: Preliminary results. Acta Hortic. 1214:165-70.

De Oliveira G.A., Bureau S., Renard C.M.G.C., Pereira-Netto A.B., De Castilhos F. 2014. Comparison of NIRS approach for prediction of internal quality traits in three fruit species. Food Chem. 143:223-30.

ElMasry G., Wang N., ElSayed A., Ngadi M. 2007. Hyperspectral imaging for nondestructive determination of some quality attributes for strawberry. J. Food Engine. 81:98-107.

Guo W., Li W., Yang B., Zhu Z.Z., Liu D., Zhu X. 2019. A novel noninvasive and cost-effective handheld detector on soluble solids content of fruits. J. Food Engine. 257:1-9.

Helin R., Indahl U.G., Tomic O., Liland K.H. 2021. On the possible benefits of deep learning for spectral preprocessing. J. Chemometr. 36:e3374.

Manley M., Joubert E., Myburgh L., Kidd M. 2007. Prediction of soluble solids content and post-storage internal quality of Bulida apricots using near infrared spectroscopy. J. Near Infrared Spectros. 15:179-88.

McGlone V.A., Kawano S. 1998. Firmness, dry-matter and soluble-solids assessment of postharvest kiwifruit by NIR spectroscopy. Postharv. Biol. Technol. 13:131-41.

Munera S., Besada C., Blasco J., Cubero S., Salvador A., Talens P., Aleixos N. 2017. Astringency assessment of persimmon by hyperspectral imaging. Postharv. Biol. Technol. 125:35-41.

Nicolaï B.M., Beullens K., Bobelyn E., Peirs A., Saeys W., Theron K.I., Lammertyn J. 2007. Nondestructive measurement of fruit and vegetable quality by means of NIR spectroscopy: A review. Postharv. Biol. Technol. 46:99-118.

Pu H., Liu D., Wang L., Sun D.W. 2016. Soluble solids content and ph prediction and maturity discrimination of Lychee fruits using visible and near infrared hyperspectral imaging. Food Analyt. Methods. 9:235-44.

Ruiz D., Reich M., Bureau S., Renard C.M.G.C., Audergon J.M. 2008. Application of reflectance colorimeter measurements and infrared spectroscopy methods to rapid and nondestructive evaluation of carotenoids content in apricot (Prunus armeniaca L.). J. Agric. Food Chem. 56:4916-922.

Uwadaira Y., Sekiyama Y., Ikehata A. 2017. An examination of the principle of non-destructive flesh firmness measurement of peach fruit by using VIS-NIR spectroscopy. Heliyon. 4:e00531.

Wendel A., Underwood J., Walsh K. 2018. Maturity estimation of mangoes using hyperspectral imaging from a ground based mobile platform. Comput. Electron. Agric. 155:298-313.

Witherspoon J.M., Jackson J.F. 1995. Analysis of fresh and dried apricot. In: Linskens H.F., Jackson J.F. (Eds.), Fruit analysis. Modern methods of plant analysis, Vol. 18. Springer-Verlag, Berlin-Heidelberg, Germany, pp. 111-131.

Xue J, Zhang S, Zhang J, 2015. Ripeness classification of Shajin apricot using hyperspectral imaging technique. Nongye Gongcheng Xuebao/Trans. Chinese Soc. Agric. Engine. 31:300-7.